Inorg. Chem. **2002**, *41*, 367–378

Novel Ruthenium Sensitizers Containing Functionalized Hybrid Tetradentate Ligands: Synthesis, Characterization, and INDO/S Analysis

T. Renouard, R.-A. Fallahpour,[†] Md. K. Nazeeruddin,* R. Humphry-Baker, S. I. Gorelsky,[‡] A. B. P. Lever,*[,‡] and M. Grätzel*

Laboratory for Photonics and Interfaces, Institute of Physical Chemistry, Swiss Federal Institute of Technology, CH-1015 Lausanne, Switzerland, and Department of Chemistry, York University, 4700 Keele Street, Toronto, Ontario, Canada M3J 1P3

Received May 15, 2001

Ruthenium sensitizers of the type *trans*-[Ru(**L**^{1})(X)$_2$], *trans*-[Ru(**L**^{2})(X)$_2$], *trans*-[Ru(**L**^{3})(X)$_2$], and *trans*-[Ru(**L**^{4})(X)$_2$] (where **L**^{1} = 6,6′-bis(1-*H*-benzimidazol-2-yl)-4,4′-bis(methoxycarbonyl)-2,2′-bipyridine, **L**^{2} = 4,4‴-bis(*tert*-butyl)-4′,4″-bis[*p*-(methoxycarbonyl)phenyl]-2,2′:6′,2″:6″,2‴-quaterpyridine, **L**^{3} = 4′,4″-bis[3,4-(dimethoxy)phenyl]-2,2′:6′,2″:6″,2‴-quaterpyridine, and **L**^{4} = 4′,4″-diethoxycarbonyl-2,2′:6′,2″:6″,2‴-quaterpyridine; X = Cl$^-$, NCS$^-$) were synthesized and characterized by CV, NMR, and UV–vis absorption and emission spectroscopy. The *trans*-dichloro and dithiocyanate complexes show MLCT transitions in the entire visible and near-IR region. The lowest energy metal-to-ligand charge-transfer transition band of the *trans*-dichloro complexes is around 14 300 cm^{-1} in DMF solution, and these complexes show weak and broad emission signals with onset at above 10 500 cm^{-1}. The absorption and emission maxima of the *trans*-dithiocyanate complexes are blue-shifted compared to those of its *trans*-dichloro analogues because of the strong π acceptor property of the NCS$^-$ compared to the Cl$^-$. The electronic spectra of *trans*-[Ru(L)(X)$_2$] complexes were calculated by INDO/S and compared with the experimental data. The extent of mixing between metal 4d and ligand π* orbitals is discussed. Extensive π-back-donation is observed. The panchromatic response of these novel complexes renders them as suitable sensitizers for solar energy conversion applications based on titanium dioxide mesoporous electrodes. Preliminary results using the *trans*-[Ru(**L**^{4})(NCS)$_2$] complex show 75% incident photon-to-current efficiencies (IPCE), yielding 18 mA/cm^2 current density under standard AM 1.5 sunlight.

1. Introduction

Ruthenium polypyridine complexes are well established as photosensitizers for use in photovoltaic cells based on nanocrystalline TiO_2 films.[1−9] The widely used and most efficient heterogeneous charge-transfer sensitizer in the nanocrystalline TiO_2 solar cell is the *cis*-dithiocyanato-bis-(2,2′-bipyridyl-4,4′-dicarboxylate) ruthenium(II) complex (referred to as N3). Using N3 as a charge-transfer sensitizer,

* Authors to whom correspondence should be addressed. E-mail: Mdkhaja.Nazeeruddin@epfl.ch (Md.K.N.).

[†] Institute of Inorganic Chemistry, University of Basel, Spitalstrasse 51, Basel, Switzerland.

[‡] York University.

(1) Grätzel, M. *Prog. Photovoltaics* **2000**, *8*, 171. (b) *Future Generation Photovoltaic Technologies*; McConnell, R. D., Ed.; American Institute of Physics Conference Proceedings 404, Denver, CO, 1997.

(2) Schlichthörl, G.; Park, N. G.; Frank, A. J. *J. Phys. Chem. B* **1999**, *103*, 782. (b) Huang, S. Y.; Schlichthörl, G.; Nozik, A. J.; Grätzel, M.; Frank, A. J. *J. Phys. Chem. B* **1997**, *101*, 2576. (c) Schlichthorl, G.; Huang, S. Y.; Frank, A. J. *J. Phys. Chem. B* **1997**, *101*, 8141.

(3) Zaban, A.; Ferrrere, S.; Sprague, J.; Gregg, B. A. *J. Phys. Chem. B.* **1997**, *101*, 55. (b) Ferrrere, S.; Gregg, B. A. *J. Am. Chem. Soc.* **1998**, *120*, 843. (c) Lemon, B. I.; Hupp, J. T. *J. Phys. Chem. B* **1999**, *103*, 3797. (d) Langdon, B. T.; MacKenzie, V. J.; Asunskis, D. J.; Kelly, D. F. *J. Phys. Chem. B* **1999**, *103*, 11176.

(4) Kelly, C. A.; Farzad, F.; Thompson, D. W.; Stipkala, J. M.; Meyer, G. J. *Langmuir* **1999**, *15*, 7047. (b) Thompson, D. W.; Kelly, C. A.; Farzad, F.; Meyer, G. J. *Langmuir* **1999**, *15*, 650.

(5) Schwarzburg, K.; Willig, F. *J. Phys. Chem. B* **1999**, *103*, 5743. (b) Franco, G.; Gehring, J.; Peter, L. M.; Ponomarev, E. A.; Uhlendorf, I. *J. Phys. Chem. B* **1999**, *103*, 692. (c) Salafsky, J. S.; Lubberhuizen, W. H.; van Faassen, E.; Schropp, R. E. I. *J. Phys. Chem. B* **1998**, *102*, 766.

(6) Solbrand, A.; Henningsson, A.; Södergren, S.; Lindström, H.; Hagfeldt, A.; Lindquist, S.-E. *J. Phys. Chem. B* **1999**, *103*, 1078.

(7) Bando, K. K.; Mitsuzuka, Y.; Sugino, M.; Sughihara, H.; Sayama, K.; Arakawa, H. *Chem. Lett.* **1999**, 853. (b) Sughihara, H.; Sing, L. P.; Sayama, K.; Arakawa, H.; Nazeeruddin, Md. K.; Grätzel, M. *Chem. Lett.* **1998**, 1005. (c) Sayama, K.; Sughihara, H.; Arakawa, H. *Chem. Mater.* **1998**, *10*, 3825. (d) Murakoshi, K.; Kano, G.; Wada, Y.; Yanagida, S.; Miyazaki, H.; Matsumoto, M.; Murasawa, S. *J. Electroanal. Chem.* **1995**, *396*, 27.

(8) Argazzi, R.; Bignozzi, C. A.; Heimer, T. A.; Meyer, G. J. *Inorg. Chem.* **1997**, *36*, 2. (b) Argazzi, R.; Bignozzi, C. A.; Hasselmann, G. M.; Meyer, G. J. *Inorg. Chem.* **1998**, *37*, 4533.

10.1021/ic010512u CCC: $22.00
Published on Web 01/03/2002

we, and others, have obtained incident photon-to-current conversion efficiencies (IPCEs) of 80−85%.[10] The electron injection rates of this complex have been measured in different laboratories and were found to occur in the femtosecond time scale.[11] However, the main drawback of this sensitizer is the lack of absorption in the red region of the visible spectrum, a factor which needs to be addressed.

The optimal sensitizer for the dye-sensitized solar cell should be panchromatic, that is, absorb visible light of all colors. Ideally, all photons below a threshold wavelength of about 920 nm should be harvested and converted to electric current.[12] To absorb the light below 920 nm, the redox level (energy levels) of the sensitizer needs to be tuned. The metal-to-ligand charge-transfer transitions can be tuned to lower energy in two ways: first, by introducing a ligand with a low lying π^* molecular orbital, and second, by the destabilization of the metal t_{2g} orbitals with a strong donor ligand. Meyer et al. have used these strategies successfully to tune the MLCT transitions in ruthenium complexes.[13] The design of such molecules can be facilitated by the use of ligand electrochemical parameter theory as noted.[14,15] Heteroleptic complexes containing bidentate ligands with low lying π^* orbitals together with others having strong σ-donating properties indeed show impressive absorption properties.[16]

Geometrical isomerization (*cis*-to-*trans*) is another interesting and exciting approach for tuning the spectral properties of metal complexes. The absorption spectral data have been reported for several *trans*-ruthenium-polypyridine complexes whose lowest energy MLCT transitions are significantly red-shifted compared to their analogous *cis* complexes.[17] Nevertheless, a drawback of the use of the *trans* complexes is their thermal and photoinduced isomerization back to the *cis* configuration.[18]

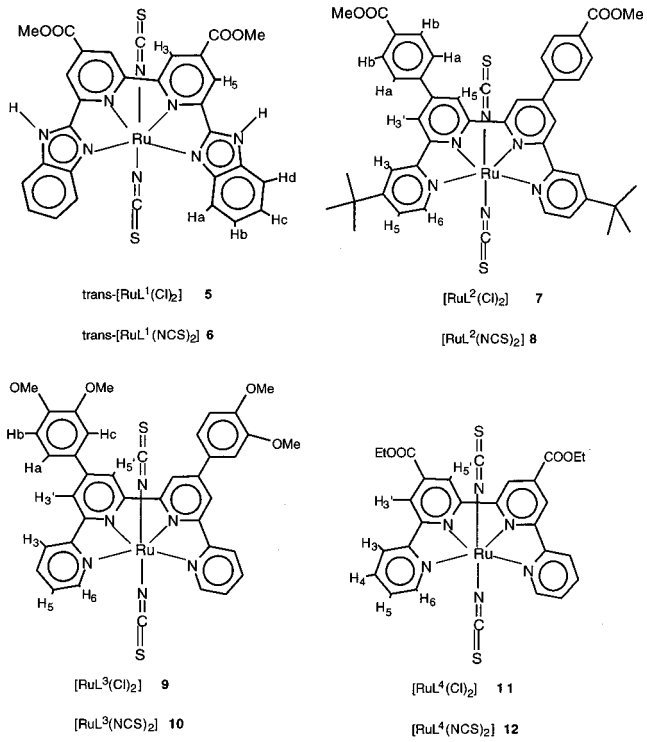

Figure 1. Hydrogen numbering for the ^{1}H NMR assignment of complexes **5**−**12**.

In an effort to stabilize the *trans* configuration of an octahedral ruthenium complex and integrate the concepts of donor and acceptor in a single complex, we have engineered at a molecular level and synthesized functionalized hybrid tetradentate ligands and their ruthenium complexes (Figure 1), which are expected to show thermal stability and photostability. The donor units of the tetradentate ligand (benzimidazole in $\mathbf{L^1}$, and *tert*-butylpyridine in $\mathbf{L^2}$) tune the metal t_{2g} orbital energies, and the acceptor units (methoxycarbonyl) tune the π^* molecular orbitals. The application of a tetradentate ligand will inhibit the *trans* → *cis* isomerization process. The axial coordination sites are used further to fine-tune the spectral and redox properties and to stabilize the hole that is being generated on the metal, after having injected an electron into the conduction band.

In this paper, we describe four novel ligands and their ruthenium complexes, INDO/S analysis of the UV−vis spectra, and incident photon-to-current efficiency data.

2. Experimental Section

Materials. The solvents, potassium thiocyanate, ammonium thiocyanate, and tetrabutylammonium thiocyanate were supplied from Fluka. $[Ru(p\text{-cymene})Cl_2]_2$ was purchased from Aldrich. Deuterated solvents were obtained from Dr. Glaser A.G. The reagents were of puriss grade quality and used without further

(9) Tennakone, K.; Kumara, G. R. R. A.; Kottegoda, I. R. M.; Perera, V. P. S. *Chem. Commun*. **1999**, 15. (b) Nasr, C.; Hotchandani, S.; Kamat, P. V. *J. Phys. Chem. B* **1998**, *102*, 4944−4951. (c) Ihara, M.; Tanaka, K.; Sakaki, K.; Honma, I.; Yamada, K. *J. Phys. Chem. B* **1997**, *101*, 5153. (d) Jing, B.; Zhang, H.; Zhang, M.; Lu, Z.; Shen, T. *J. Mater. Chem*. **1998**, *8*, 2055.

(10) Nazeeruddin, Md. K.; Kay, A.; Rodicio, I.; Humphry-Baker, R.; Muller, E.; Liska, P.; Vlachopoulos, N.; Grätzel, M. *J. Am. Chem. Soc*. **1993**, *115*, 6382. (b) Nazeeruddin, Md. K.; Pechy, P.; Renouard, T.; Zakeeruddin, S. M.; Humphry-Baker, R.; Liska, P.; Cevey, L.; Costa, E.; Shklover, V.; Spiccia, L.; Deacon, G.; Bignozzi, C. A.; Grätzel, M. *J. Am. Chem. Soc.* **2001**, *123*, 1613. (c) Hou, Y.-J.; Xie, P.-H.; Zhang, B.-W.; Cao, Y.; Xiao, X.-R.; Wang, W.-B. *Inorg. Chem.* **1999**, *38*, 6320.

(11) Asbury, J. B.; Ellingson, R. J.; Ghosh, H. N.; Ferrere, S.; Nozik, A. J.; Lian, T. *J. Phys. Chem. B* **1999**, *103*, 3110. (b) Moser, J. E.; Noukakis, D.; Bach, U.; Tachibana, Y.; Klug, D. R.; Durrant, J. R.; Humphry-Baker, R.; Grätzel, M. *J. Phys. Chem. B* **1998**, *102*, 3649. (c) Haque, S. A.; Tachibana, Y.; Klug, D. R.; Durrant, J. R. *J. Phys. Chem. B* **1998**, *102*, 1745.

(12) Haught, A. F. *J. Sol. Energy Eng.* **1984**, *106*, 3. (b) Winter, C.; Sizman, R.; Vant Hull, L. *Solar Power Plants*; Springer-Verlag: New York, 1991; Chapter 2. (c) De Vos, A. *Endoreversible Thermodynamics of Solar Energy Conversion*; Oxford Science Publishers: Oxford, 1992; Chapter 6. (d) Luque, A.; Araujo, G. *Physical limitations to photovoltaic conversion*; Adam Hilger: New York, 1990; p 106. (e) Baruch, P. *J. Appl. Phys*. **1985**, *57*, 1347.

(13) Treadway, J. A.; Moss, J. A.; Meyer, T. J. *Inorg. Chem*. **1999**, *38*, 4386. (b) Alebbi, M.; Bignozzi, C. A.; Heimer, T. A.; Hasselmann, G. M.; Meyer, G. J. *J. Phys. Chem. B* **1998**, *102*, 7577.

(14) Lever, A. B. P. *Inorg. Chem.* **1990**, *29*, 1271.

(15) Lever, A. B. P.; Dodsworth, E. S. In *Inorganic Electronic Structure and Spectroscopy*; Solomon, E. I., Lever, A. B. P., Eds.; Wiley-Interscience: New York, 1999; Vol. 2, p 227.

(16) Anderson, P. A.; Strouse, G. F.; Treadway, J. A.; Keene, F. R.; Meyer, T. J. *Inorg. Chem*. **1994**, *33*, 3863.

(17) Durham, B.; Wilson, S. R.; Hodges, D. J.; Meyer, T. J. *J. Am. Chem. Soc.* **1980**, *102*, 600. (b) Masood, M. A.; Sullivan, B. P.; Hodges, D. J. *Inorg. Chem.* **1994**, *33*, 5360. (c) Walsh, J. L.; Durham, B. *Inorg. Chem.* **1982**, *21*, 329.

(18) Hesek, D.; Inoue, Y.; Everitt, R. L. *Chem. Lett.* **1999**, 109. Tse, Y.-H.; Auburn, P. R.; Lever, A. B. P. *Can. J. Chem.* **1992**, *70*, 1849.

purification, unless specified. Hydrated ruthenium trichloride was purchased from Johnson Matthey and used as received. Sephadex LH-20 (Pharmacia) material was allowed to swell in water for 2 h before filling into a column.

Analytical Measurements. Elemental analyses were performed at Iise Beetz, Mikroanalytisches Laboratorium, Germany. UV−vis and fluorescence spectra were recorded in a 1 cm path length quartz cell on a Cary 5 spectrophotometer and a Spex Fluorolog 112 spectrofluorimeter, respectively. The emitted light was detected with a Hamamatsu R2658 photomultiplier operated in single photon counting mode. The emission spectra were photometrically corrected using a calibrated 200 W tungsten lamp as reference source. The emission lifetimes were measured by exciting the sample with a pulse from an active mode locked Nd:YAG laser, using the frequency doubled line at 532 nm. The emission decay was followed on a Tektronix DSA 640 digitizing signal analyzer, using a Hamamatsu R928 photomultiplier to convert the light signal to a voltage waveform.

Electrochemical data were obtained by cyclic voltammetry using a three-electrode cell and a BAS100 electrochemical analyzer. The working electrode was a 0.07 cm^2 glassy carbon disk, the auxiliary electrode was a glassy carbon rod, the reference electrode was AgCl/Ag, saturated KCl (0.197 V vs SHE), and the supporting electrolyte was 0.1 M tetrabutylammonium tetrafluoroborate (TBATFB).

^1H and ^{13}C NMR spectra were measured with a Bruker ACP-200 spectrometer at 200 MHz and 50.3 MHz, respectively. The reported chemical shifts were against TMS. The ATR-FTIR spectra were measured using a Nicolet 510 FTIR spectrometer equipped with a "Golden Gate (TM)" (Graseby-Specac) single reflection diamond-ATR accessory. The IR bench was flushed with nitrogen gas, and the spectra are the average of 50 accumulated scans.

Photoelectrochemical Measurements. Photoelectrochemical data were measured using a 450 W xenon light source that was focused to give 1000 W/m^2, the equivalent of one sun at AM 1.5, at the surface of the test cell. The spectral output of the lamp was matched in the region 350−750 nm with the aid of a Schott KG-5 sunlight filter so as to reduce the mismatch between the simulated and the true solar spectrum to less than 2%. The differing intensities were regulated with neutral wire mesh attenuators. The applied potential and measured cell current was measured using a Keithley Model 2400 digital source meter. The current−voltage characteristics of the cell under these conditions were determined by biasing the cell externally and measuring the generated photocurrent. This process was fully automated using Wavemetrics software. A similar data acquisition system was used to control the incident photon-to-current conversion efficiency (IPCE) measurement. Under full computer control, light from a 300 W Xe lamp was focused through a high throughput monochromator onto the photovoltaic cell under test. The monochromator was incremented through the visible spectrum to generate the IPCE(λ) curve as defined by the following equation:

$$\mathrm{IPCE}(\lambda) = 1240(I_{sc}/\lambda\phi)$$

where λ is the wavelength, I_{sc} is the current at short circuit (mA/cm^2), and ϕ is the incident radiative flux (W/m^2). This curve can be derived from the measured absorption spectrum of the adsorbed photosensitizer for comparison.

TiO_2 Electrode Preparation. The TiO_2 colloidal paste was prepared using published procedures.[10b] The TiO_2 paste is deposited onto sheet glass (Nippon Sheet Glass, Hyogo, Japan; glass has been coated with a fluorine-doped stannic oxide layer, sheet resistance of 8−10 Ω/cm^2) using a screen printing technique. The resulting layer is dried in air at 100 °C for 15 min followed by another 15 min at 150 °C. For the final processing, the layers were heated using a titanium hot plate (Bioblock Scientific) to 325 °C at a rate of 30 °C/min and kept at this temperature for 5 min. Then, the temperature was raised to 375 °C at a rate of 10 °C/min and held there for 5 min. Finally, the layers were fired to 450 °C at a rate of 15 °C/min under flowing oxygen and left at this temperature for 20 min before cooling to room temperature.

The heated electrodes were impregnated with a 0.05 M titanium tetrachloride solution in a water saturated desiccator for 30 min at 70 °C and washed with distilled water. The 0.05 M titanium tetrachloride solution was prepared in the following manner: First, 2 M titanium tetrachloride solution was prepared by adding directly titanium tetrachloride liquid into a bottle containing ice, which was cooled to −20 °C, and then the solution was further diluted to 0.05 M.

3. Synthesis

(1) Synthesis of 6,6′-Bis(1-*H*-benzimidazol-2-yl)-4,4′-bis-(methoxycarbonyl)-2,2′-bipyridine (L^1). (1.1) 4,4′-Bis(ethoxy-carbonyl)-2,2′-bipyridine-*N*,*N*′-dioxide. To a solution of 4,4′-bis(ethoxycarbonyl)-2,2′-bipyridine (2 g, 6.6 mmol) in acetic acid (20 mL) was added peracetic acid (4 mL, 24 mmol) dropwise. The reaction mixture was stirred at 40 °C for 3 days and then cooled to room temperature, 25 °C.[19] The excess peracetic acid was neutralized by slow addition of dimethyl sulfide (2.5 mL), and the solvents were evaporated to dryness. The resulting mixture was added to cold methanol (50 mL), resulting in a white precipitate, which was filtered off and washed with cold methanol to yield the title compound as white needles (2.1 g; 95%). ^1H NMR ($CDCl_3$, δ ppm, J Hz): 8.36 (2H, dd, $H^{6,6'}$, J = 6.8, 0.4); 8.18 (2H, dd, $H^{3,3'}$, J = 2.5, 0.4); 7.99 (2H, dd, $H^{5,5'}$, J = 6.8, 2.5); 4.42 (4H, q, CH_2, J = 7.1); 1.41 (6H, t, CH_3, J = 7.1).

(1.2) 6,6′-Dicyano-4,4′-bis(ethoxycarbonyl)-2,2′-bipyridine. A solution of freshly distilled dimethyl sulfate (5 mL) and 4,4′-bis-(ethoxycarbonyl)-2,2′-bipyridine-*N*,*N*′-dioxide (0.66 g, 2 mmol) was warmed at 100 °C for 4 h. Then, the reaction mixture was allowed to cool to room temperature, 25°C, which resulted in a viscous liquid. The viscous liquid was added dropwise to a saturated aqueous potassium cyanide solution (during the addition, the potassium cyanide solution was stirred vigorously, and the temperature was maintained at −10 °C). During the course of addition, a fawn-colored solid developed, which was stirred for another 4 h at −10 °C. Then, the reaction mixture was placed at −20 °C for 15 h, and the resulting brownish precipitate was filtered and washed with water. Using this brownish precipitate, the reaction was repeated for a second time; that is, the brownish precipitate was again taken in 5 mL of distilled dimethyl sulfate and warmed at 100 °C for 4 h and then treated with potassium cyanide solution as described. The resulting precipitate was dissolved in a small amount of dichloromethane and precipitated by slow addition to methanol (50 mL) to yield the title compound as a white powder (0.38 g, 55%). ^1H NMR ($CDCl_3$, δ ppm, J Hz): 9.20 (2H, d, $H^{3,3'}$, J = 1.4); 8.36 (2H, d, $H^{5,5'}$, J = 1.4); 4.55 (4H, q, CH_2, J = 7.1); 1.50 (6H, t, CH_3, J = 7.1).

(1.3) 6,6′-Bis(1-*H*-benzimidazol-2-yl)-4,4′-bis(methoxycarbo-nyl)-2,2′-bipyridine (L^1). Sodium methylate (62 mg, 1.0 mmol) and 6,6′-dicyano-4,4′-bis(ethoxycarbonyl)-2,2′-bipyridine (175 mg, 0.5 mmol) were heated at 60 °C in freshly distilled methanol (40 mL) for 6 h. To this solution was added *o*-phenylenediamine

(19) Oki, A. R.; Morgan, R. J. *Synth. Commun.* **1995**, *25*, 4093. (b) Ishikawa, O.; Ren, Z. *J. Pharm. Soc. Jpn.* **1944**, *64*, 73.

dihydrochloride (0.2 g, 1.0 mmol). The solution turned yellow and then formed a precipitate, which was stirred at 60 °C for 12 h. After cooling to room temperature (25 °C), the solution was treated with aqueous sodium carbonate. The precipitate was filtered and washed with methanol to yield the title compound as a pale yellow powder (170 mg, 67%). ^{1}H NMR (DMSO-d_6, δ ppm, J Hz): 9.28 (2H, d, H$^{3,3'}$, J = 1.4); 8.86 (2H, d, H$^{5,5'}$, J = 1.4); 7.75 (4H, m, Ar−H); 7.31 (4H, m, Ar−H); 4.07 (6H, s, CH_3).

Anal. Found: C, 60.28; H, 4.65; N, 15.36%. Calcd for $C_{28}H_{20}N_6O_4 \cdot 3H_2O$: C, 60.21; H, 4.69; N, 15.04%.

(2) Synthesis of 4,4‴-Bis(*tert*-butyl)-4′,4″-bis[*p*-(methoxycarbonyl)phenyl]-2,2′:6′,2″:6″,2‴-quaterpyridine (L^2). (2.1) 1,6-Bis[*p*-(methoxycarbonyl)phenyl]hexa-1,5-diene-3,4-dione. Piperidine (0.5 mL, 5 mmol) and acetic acid (0.3 mL, 5 mmol) were added to a stirred solution of methyl 4-formylbenzoate (1.55 g, 9 mmol) and 2,3-butanedione (0.4 mL, 4.5 mmol) in methanol (15 mL). The mixture was refluxed for 6 h, during which bright orange crystals started to form. After cooling to room temperature, the crystals were filtered and washed with methanol to yield the title compound (0.42 g, 25%). ^{1}H NMR (DMSO-d_6, δ ppm, J Hz): 8.03 (4H, d, Ar−H, J = 8.0); 7.95 (4H, d, Ar−H, J = 8.0); 7.84 (2H, d, ═CH, J = 16.0); 7.50 (2H, d, ═CH, J = 16.0); 3.88 (6H, s, CH_3).

(2.2) *N*-{2-oxo-2-[2-(4-*tert*-butyl)pyridyl]ethyl}pyridinium Iodide. 2-Acetyl-4-*tert*-butylpyridine (1.6 g, 9 mmol) was added to a solution of iodine (5 g, 20 mmol) in anhydrous pyridine (20 mL), and the mixture was heated at 70 °C for 1 h. The dark solution was cooled to room temperature and the solvent evaporated. To the resulting mixture was added dichloromethane. After filtration and evaporation, the title compound was collected as fine brownish crystals (0.94 g, 66%). ^{1}H NMR ($CDCl_3$, δ ppm, J Hz): 9.01 (2H, d, H$^{2',6'}$, J = 6.6); 8.78 (1H, dd, H,^{6} J = 5.1, 0.55); 8.28 (2H, d, H$^{3',5'}$, J = 6.6); 8.15 (1H, d, H$^{4'}$, J = 7.7); 8.02 (1H, dd, H^3, J = 1.2, 0.55); 7.85 (1H, dd, H,^{5} J = 5.1, 1.2); 6.51 (2H, s, CH_2); 1.34 (9H, s, ^{t}Bu).

(2.3) 4,4‴-Bis(*tert*-butyl)-4′,4″-bis[*p*-(methoxycarbonyl)-phenyl]-2,2′:6′,2″:6″,2‴-quaterpyridine. 1,6-Bis[*p*-(methoxycarbonyl)phenyl]hexa-1,5-diene-3,4-dione (1.65 g, 4.3 mmol), *N*-{2-oxo-2-[2-(4-*tert*-butyl)pyridyl]ethyl}pyridinium iodide (3.5 g, 9.2 mmol), and ammonium acetate (1 g, 13 mmol) were refluxed in ethanol (25 mL) for 12 h. The mixture was cooled to room temperature, and the precipitate which formed was filtered and washed with ethanol to yield the title compound as a brownish powder (0.68 g, 23%). ^{1}H NMR ($CDCl_3$, δ ppm, J Hz): 9.06 (2H, d, H$^{3',5''}$, J = 1.6); 8.82 (2H, d, H$^{5',3''}$, J = 1.6); 8.81 (2H, d, H$^{3,3'''}$, J = 1.4); 8.68 (2H, d, H$^{6,6'''}$, J = 5.3); 8.24 (4H, d, Ar−H, J = 8.5); 8.05 (4H, d, Ar−H, J = 8.5); 7.42 (2H, dd, H$^{5,5'''}$, J = 5.3, 1.9); 4.00 (6H, s, CH_3); 1.49 (18H, s, ^{t}Bu).

Anal. Found: C, 76.53; H, 6.10; N, 8.05%. Calcd for $C_{44}H_{42}N_4O_4$: C, 76.49; H, 6.12; N, 8.11%.

(3) Synthesis of 4′,4″-bis[3,4-(dimethoxy)phenyl]-2,2′:6′,2″:6″,2‴-quaterpyridine (L^3). Using the same conditions as for compound **L^2**, starting from 1,6-bis[3,4-(dimethoxy)phenyl]hexa-1,5-diene-3,4-dione (1.5 g, 4. mmol) and *N*-[2-oxo-2-(2-pyridyl)-ethyl]pyridinium iodide (3.5 g, 9.2 mmol), the title compound was obtained as a pale yellow powder (475 mg, 21%). ^{1}H NMR ($CDCl_3$, ppm, J Hz): 8.91 (2H, d, H$^{3',5''}$, J = 1.7); 8.78 (2H, m, H$^{3,3'''}$); 8.75 (2H, m, H$^{5',3''}$); 8.71 (2H, m, H$^{6,6'''}$); 7.94 (2H, dd, H$^{4,4'''}$, J = 7.7, 1.6); 7.55 (2H, d, Ar−H, J = 8.3, 2.0); 7.46 (2H, d, Ar−H, J = 2.0); 7.41 (2H, dd, H$^{5,5'''}$, J = 7.4, 1.5); 7.07 (2H, d, Ar−H, J = 8.3); 4.06 (6H, s, CH_3); 4.00 (6H, s, CH_3).

Anal. Found: C, 74.30; H, 5.35; N, 9.46%. Calcd for $C_{36}H_{30}N_4O_4$: C, 74.21; H, 5.20; N, 9.61%.

(4) 4′,4″-Diethoxycarbonyl-2,2′:6′,2″:6″,2‴-quaterpyridine (L^4). Tetrahydrofuran (20 mL) was added to a mixture of $NiBr_2$-$(PPh_3)_2$ (100 mg, 0.144 mmol), zinc (120 mg, 1.89 mmol), and tetraethylammonium iodide (Et_4NI, 60 mg, 0.233 mmol) under nitrogen at room temperature. The resulting green color of the solution changed gradually to dark red. Ethyl-6-bromo-2,2′-bipyridine-4′-carboxylic ester (70 mg, 0.23 mmol)[20] was separately dissolved in THF and added to the above solution by syringe. After stirring for 16 h at 50 °C, the mixture was poured into 2 M aqueous ammonia solution (60 mL). To the resulting mixture was added chloroform (100 mL). The organic layer was separated, and the aqueous phase was extracted with chloroform (3 × 30 mL). The combined organic phases were washed with water (5 × 50 mL) and saturated NaCl solution (50 mL). The organic layer was dried ($MgSO_4$), and solvent was removed. To the resulting residue was added concentrated hydrochloric acid (20 mL), and then, the material was extracted with dichloromethane (3 × 30 mL). The aqueous phase was cautiously neutralized with solid sodium carbonate. After extraction with dichloromethane (4 × 40 mL), the combined organic phases were dried ($MgSO_4$) and the solvent was removed. Compound **L^4** was then purified on silica gel with 3/2 dichloromethane/hexane. Yield: 30 mg (58%). ^{1}H NMR ($CDCl_3$): δ 9.16 (2H, d, J = 1.50, H$^{3'}$); 9.03 (2H, d, J = 1.50, H$^{5'}$); 8.75 (2H, m, H^6); 8.71 (2H, md, J = 7.80, H^3); 7.92 (2H, ddd, J = 8.30, J = 7.80, J = 1.95, H^4); 7.39 (2H, ddd, J = 8.30, J = 7.80, J = 1.95, H^5); 4.52 (4H, q, J = 6.90, CH_2); 1.50 (6H, t, J = 6.90, CH_3).

Anal. Found: C, 68.64; H, 5.01; N, 12.26%. Calcd for $C_{26}H_{22}N_4O_4$: C, 68.71; H, 4.88; N, 12.33%.

(5) Synthesis of Ru(L^1)Cl$_2$. [Ru(*p*-cymene)Cl_2]$_2$ (61 mg, 0.1 mmol) was dissolved in ethanol (50 mL) by heating. To this orange solution was added ligand **L^1** (100 mg, 0.2 mmol), and the mixture was refluxed for 6 h. The black precipitate which formed was filtered and washed with ethanol to yield the title compound as a dark powder (120 mg, 90%). ^{1}H NMR (DMSO-d_6, δ ppm, J Hz): 9.12 (4H, broad s, H^3, H^5); 8.49 (2H, d, Ha, J = 8); 7.92 (2H, d, Hd, J = 7); 7.69 (4H, m, Hb, Hc); 4.10 (6H, s, CH_3).

Anal. Found: C, 49.08; H, 3.07; N, 11.88%. Calcd for $C_{28}H_{20}N_6O_4Cl_2Ru$: C, 49.66; H, 2.98; N, 12.41%.

(6) Synthesis of Ru(L^1)(SCN)$_2$. To a solution of complex **5** (42 mg, 6 × 10^{-5} mol) in DMF (35 mL) was added ammonium thiocyanate (350 mg, 4.6 mmol) in water (15 mL). The reaction mixture was heated at 140 °C for 3 h. The solution was allowed to cool to room temperature. The black precipitate which formed was filtered, washed thoroughly with water, and dried under vacuum to yield the title compound as a dark powder (10 mg, 23%). The resulted crude complex was further purified using a Sephadex LH-20 column. ^{1}H NMR (DMSO-d_6, δ ppm, J Hz): 9.32 (2H,s, H^3); 9.05 (2H, s, H^5); 8.42 (2H, d, Ha, J = 8.0); 7.98 (2H, d, Hd, J = 8); 7.69 (4H, broad m, Hb, Hc), 4.10 (6H, s, CH_3).

Anal. Found: C, 49.27; H, 2.73; N, 15.25%. Calcd for $C_{30}H_{20}N_8O_4S_2Ru$: C, 49.88; H, 2.79; N, 15.51%.

(7) Synthesis of Ru(L^2)Cl$_2$. Using the same conditions as for complex **5**, starting from ligand **L^2** (120 mg, 1.8 × 10^{-4} mol), the title compound was obtained as a dark powder (130 mg, 89%). ^{1}H NMR (DMSO-d_6, δ ppm, J Hz): 9.61 (2H, d, H^6, J = 6); 9.10 (2H, d, H$^{3'}$, J = 2); 9.01 (2H, d, H$^{5'}$, J = 2); 8.78 (2H, d, H^3, J = 2); 8.36 (4H, d, Ha, J = 8.4); 8.18 (4H, d, Hb, J = 8.4); 7.90 (2H, dd, H,^{5} J = 5.7, 1.8); 3.95 (6H, s, CH_3); 1.54 (18H, s, ^{t}Bu).

Anal. Found: C, 59.58; H, 4.85; N, 6.42%. Calcd for $C_{44}H_{42}N_4O_4Cl_2Ru$: C, 61.20; H, 4.90; N, 6.48%.

(20) Fallahpour, R.-A. *Synthesis* **2000**, 1138. (b) Iyoda, M.; Otsuka, H.; Sato, K.; Nisato, N.; Oda, M. *Bull. Chem. Soc. Jpn.* **1990**, *63*, 80.

(8) Synthesis of Ru(L^2)($SCN)_2$. Using the same conditions as for complex **6**, starting from complex **7** (70 mg, 8×10^{-5} mol), the title compound was obtained as a dark powder (66 mg, 90%) and purified using a Sephadex LH-20 column. ^{1}H NMR (DMSO-d_6, δ ppm, J Hz): 9.57 (2H, d, H,[6] $J = 6$); 9.20 (2H, d, H$^{3'}$, $J = 2''$); 9.14 (2H, d, H$^{5'}$, $J = 2$); 8.86 (2H, d, H^3, $J = 2$); 8.38 (4H, d, Ha, $J = 8.5$); 8.23 (4H, d, Hb, $J = 8.5$); 7.93 (2H, dd, H,[5] $J = 5.7$, 1.8); 3.95 (6H, s, CH_3); 1.54 (18H, s, ^{t}Bu).

Anal. Found: C, 59.95; H, 4.65; N, 8.90%. Calcd for $C_{46}H_{42}N_6O_4S_2Ru$: C, 61.11; H, 4.68; N, 8.85%.

(9) Synthesis of Ru(L^3)Cl_2. Using the same conditions as for complex **5**, starting from ligand $\mathbf{L^3}$ (120 mg, 1.8×10^{-4} mol), the title compound was obtained as a dark powder (145 mg, 99%). ^{1}H NMR (DMSO-d_6, δ ppm, J Hz): 9.78 (2H, d, H^6 $J = 5$); 8.84 (4H, s, H$^{3'}$, 5$''$); 8.77 (2H, d, Ha, $J = 9$); 8.2 (2H, t, H^4, $J = 8$); 7.75 (2H, t, H,[5] $J = 7$); 7.73 (2H, d, Hb, $J = 9$); 7.66 (2H, s, Hc); 7.18 (2H, d, H^3, $J = 7$); 3.96 (6H, s, CH_3); 3.89 (6H, s, CH_3).

Anal. Found: C, 56.51; H, 4.03; N, 7.35%. Calcd for $C_{36}H_{30}N_4O_4Cl_2Ru$: C, 57.25; H, 4.00; N, 7.41%.

(10) Synthesis of Ru(L^3)($SCN)_2$. Using the same conditions as for complex **6**, starting from complex **9** (70 mg, 8×10^{-5} mol), the title compound was obtained as a dark powder (66 mg, 90%), which was further purified using a Sephadex LH-20 column. ^{1}H NMR (DMSO-d_6, δ ppm, J = Hz): 9.74 (2H, d, H^6, $J = 6.$); 8.84 (2H, s, H$^{3''}$); 8.78 (2H, s, H$^{5''}$); 8.80 (2H, d, Ha, $J = 9$); 8.28 (2H, t, H^4, $J = 8$); 7.94 (2H, t, H^5, $J = 7$); 7.76 (2H, d, Hb, $J = 9$); 7.65 (2H, s, Hc); 7.15 (2H, d, H^3, $J = 8$); 3.97 (6H, s, CH_3); 3.89 (6H, s, CH_3).

Anal. Found: C, 57.01; H, 3.88; N, 10.44%. Calcd for $C_{38}H_{30}N_6O_4S_2Ru$: C, 57.01; H, 3.78; N, 10.49%.

(11) Synthesis of Ru(L^4)Cl_2. Using the same conditions as for complex **5**, starting from ligand $\mathbf{L^4}$ (45.4 mg, 1×10^{-5} mol), the title compound was obtained as a dark powder (49 mg, 78%). This complex is insoluble at room temperature (25 °C) in DMF and DMSO to obtain spectroscopic data.

Anal. Found: C, 49.31; H, 3.7; N, 8.95%. Calcd for $C_{26}H_{22}N_4O_4Cl_2Ru$: C, 49.79; H, 3.54; N, 8.93%.

(12) Synthesis of Ru(L^4)($SCN)_2$. Using the same conditions as for complex **6**, starting from complex **11** (35 mg, 5.5×10^{-4} mol), the title compound was obtained as a dark powder (30 mg, 79%), which was further purified using a Sephadex LH-20 column. ^{1}H NMR (CD_3OD, δ ppm, J = Hz): 9.72 (2H, d, H^6, $J = 6.$); 8.99 (2H, s, H$^{3'}$); 8.93 (2H, s, H$^{5'}$); 8.70 (2H, d, H$^{3'}$, $J = 8$); 8.38 (2H, t, H^4, $J = 6$); 8.01 (2H, t, H^5, $J = 6$); 4.49 (4H, q, $J = 7$, CH_2); 1.42 (6H, t, $J = 7$, CH_3).

Anal. Found: C, 49.91; H, 3.32; N, 12.85%. Calcd for $C_{28}H_{22}N_6O_4S_2Ru$: C, 50.06; H, 3.30; N, 12.51%.

Computational Details. DFT calculations were carried out using Gaussian 98[21] running on an SGI Origin 2000 computer, while INDO/S calculations used HyperChem 5.1 (Hypercube, Florida)[22] run on a PC Pentium II 400 MHz. Becke's three parameter hybrid functional[23] with LYP correlation functional[24] (B3LYP) and an effective core potential basis set LanL2DZ[25] were employed in the DFT calculations.

The electronic spectra of [Ru(L)Cl_2] were calculated with INDO/S,[26] utilizing the Ru parameters obtained from ref 27 and Cl parameters, $I_s = 25.23$ eV, $I_p = 15.03$ eV, $\beta_s = \beta_p = -10.5$ eV, $\zeta_s = \zeta_p = 2.033$, F^2(p,p) = 5.21 eV, G^1(s,p) = 2.66 eV, γ(ss) = 11.41 eV, from ref 28 and DFT optimized structures. The overlap weighting factors $\sigma-\sigma$ and $\pi-\pi$ were set at 1.265 and 0.585, respectively.[26] The number of singly excited configurations used was 1800 (e.g., 30×30 occupied x virtual orbitals). The atomic orbital contributions to molecular orbitals were calculated using the AOMIX program (revision 4.3).[29] The absorption profiles of the complexes were calculated by the following formula:

$$\epsilon(E) = \Sigma_{(i)} a_I \exp(-2.773(E - E_i)^2/\Delta_{1/2}{}^2) \qquad a_i = 2.174 \times 10^9 f_i/\Delta_{1/2}$$

where the sum runs over all calculated transitions with energies, E_i, (cm^{-1}) and oscillator strengths, f_i. So, the total integrated intensity under each such absorption profile is equal to a sum of the oscillator strengths, $\Sigma_{(i)}$ f_i. The half-bandwidths, $\Delta_{1/2}$, were assumed to be equal to 3000 cm^{-1} for all electronic transitions.

4. Results and Discussion

(4.1) Synthetic Studies. The ligand $\mathbf{L^1}$ was synthesized in five steps starting from 4,4′-dimethyl-2,2′-bipyridine (Scheme 1). Ligands $\mathbf{L^2}$ and $\mathbf{L^3}$ were synthesized in 3 steps using Kröhnke's methodology,[30] slightly modified by Constable et al.,[31] to prepare quaterpyridines bearing phenyl rings on the central pyridine units (Scheme 2). The ligand $\mathbf{L^4}$ was obtained in 58% yield by coupling ethyl-6-bromo-2,2′-bipyridine-4′-carboxylic ester in the presence of $NiBr_2$-$(PPH_3)_2$ catalyst as illustrated in Scheme 3.

The [Ru(*p*-cymene)$Cl_2]_2$ complex was reacted with each of the $\mathbf{L^1}$, $\mathbf{L^2}$, $\mathbf{L^3}$, and $\mathbf{L^4}$ ligands in ethanol under an argon atmosphere to obtain the corresponding *trans*-dichloro species in good yield. However, refluxing in DMF solvent gave lower yields. Reaction of the *trans*-dichloro complexes with

(21) Frisch, M. J.; Trucks, G. W.; Schlegel, H. B.; Scuseria, G. E.; Robb, M. A.; Cheeseman, J. R.; Zakrzewski, V. G.; Montgomery, J. A., Jr.; Stratmann, R. E.; Burant, J. C.; Dapprich, S.; Millam, J. M.; Daniels, A. D.; Kudin, K. N.; Strain, M. C.; Farkas, O.; Tomasi, J.; Barone, V.; Cossi, M.; Cammi, R.; Mennucci, B.; Pomelli, C.; Adamo, C.; Clifford, S.; Ochterski, J.; Petersson, G. A.; Ayala, P. Y.; Cui, Q.; Morokuma, K.; Malick, D. K.; Rabuck, A. D.; Raghavachari, K.; Foresman, J. B.; Cioslowski, J.; Ortiz, J. V.; Stefanov, B. B.; Liu, G.; Liashenko, A.; Piskorz, P.; Komaromi, I.; Gomperts, R.; Martin, R. L.; Fox, D. J.; Keith, T.; Al-Laham, M. A.; Peng, C. Y.; Nanayakkara, A.; Gonzalez, C.; Challacombe, M.; Gill, P. M. W.; Johnson, B.; Chen, W.; Wong, M. W.; Andres, J. L.; Gonzalez, C.; Head-Gordon, M.; Replogle, E. S.; Pople, J. A. *Gaussian 98*, revision A.7; Gaussian, Inc.: Pittsburgh, PA, 1998.

(22) *HyperChem for Windows*, Release 5.1, Professional Version; Hypercube, Inc.: Gainesville, FL, 1997.

(23) Becke, A. D. *J. Chem. Phys*. **1993**, *98*, 5648.

(24) Lee, C.; Yang, W.; Parr, R. G. *Phys. Rev*. **1988**, *B37*, 785.

(25) Dunning, T. H., Jr.; Hay, P. J. In *Modern Theoretical Chemistry*; Schaefer, H. F., III, Ed.; Plenum: New York, 1976; Vol. 3, p 1. (b) Hay, P. J.; Wadt, W. R. *J. Chem. Phys*. **1985**, *82*, 270. (c) Hay, P. J.; Wadt, W. R. *J. Chem. Phys*. **1985**, *82*, 284. (d) Hay, P. J.; Wadt, W. R. *J. Chem. Phys*. **1985**, *82*, 299.

(26) Ridley, J.; Zerner, M. C. *Theor. Chim. Acta* **1973**, *32*, 111. (b) Ridley, J.; Zerner, M. C. *Theor. Chim. Acta* **1976**, *42*, 223. (c) Zerner, M. C.; Loew, G. H.; Kirchner, R. F.; Mueller-Westerhoff, U. T. *J. Am. Chem. Soc*. **1980**, *102*, 589. (d) Anderson, W. P.; Edwards, W. D.; Zerner, M. C. *Inorg. Chem*. **1986**, *25*, 2728. (e) Zerner, M. C. In *Reviews in Computational Chemistry*; Lipkowitz, K. B., Boyd, D. B., Eds.; VCH Publishers, Inc.: New York, 1991; Vol. 2, Chapter 8, p 313. (f) Zerner, M. C. In *Metal-Ligand Interactions*; Russo, N., Salahub, D. R., Eds.; Kluwer Academic Publishers: Amsterdam, 1996; p 493. (g) Zerner, M. C. *ZINDO program*, version 98.1; Quantum Theory Project, University of Florida: Gainesville, FL, 1998.

(27) Krogh-Jespersen, K.; Westbrook, J. D.; Potenza, J. A.; Schugar, H. J. *J. Am. Chem. Soc*. **1987**, *109*, 7025.

(28) Gorelsky, S. I.; Kotov, V. Yu. *Russ. J. Coord. Chem*. **1998**, *24*, 491.

(29) Gorelsky, S. I.; Lever, A. B. P. *AOMIX Program*, revision 4.3; York University: Ontario, Canada, 2000. Available at http://www.chem.yorku.ca/grad/SG/.

(30) Kröhnke, F. *Synthesis* **1976**, 1.

(31) Constable, E. C.; Harverson, P.; Smith, D. R.; Whall, L. A. *Tetrahedron* **1994**, *50*, 7799.

Scheme 1

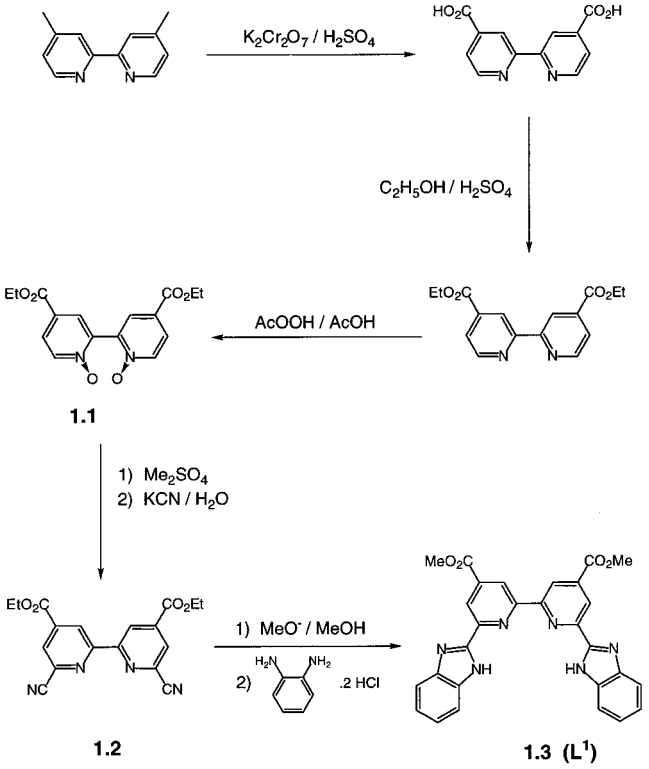

Scheme 2

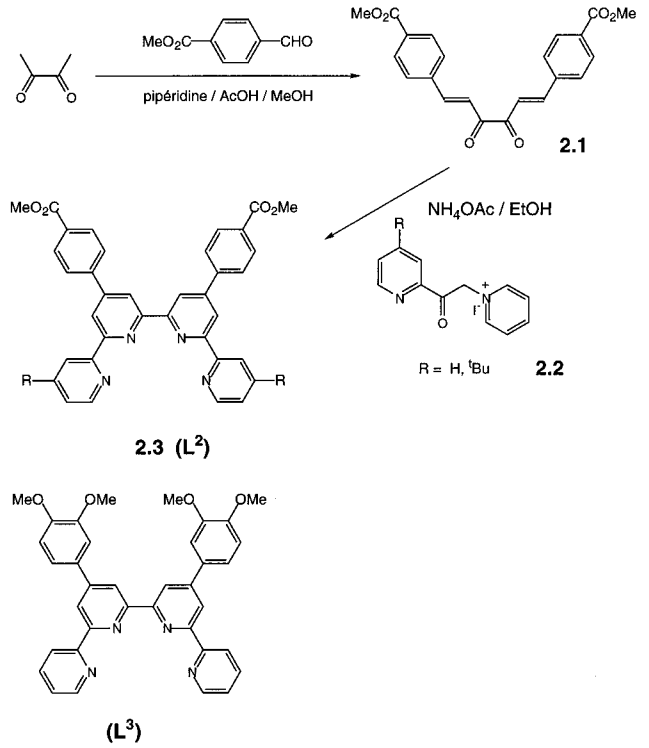

a large excess of the ambidentate thiocyanate ligand in DMF and water solution resulted in a mixture of linkage isomers. The major isomer (about 95%) is the complex with two N-bonded isothiocyanates. The isomer ratios were estimated by integrating the H-6 ^{1}H NMR signals, where the isomers show distinctly different positions.[32] These isomers were separated on a Sephadex LH-20 column using an eluent

Scheme 3

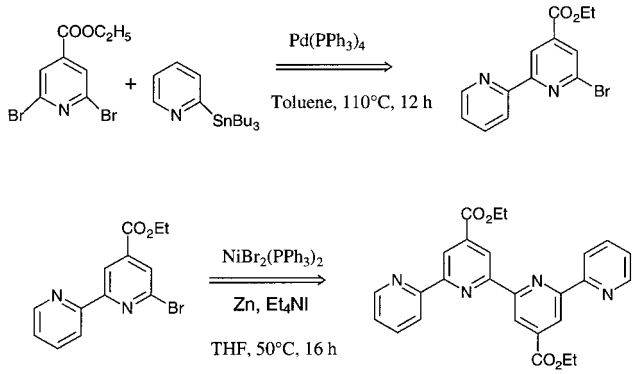

consisting of 1:5 DMF/methanol mixture. The spectroscopic data of the complexes are consistent with the proposed structures. However, in some complexes, the C, H, and N analysis data are in poor agreement with calculated values.

(4.2) NMR Spectroscopy Studies. The ^{1}H NMR spectra of the ligands show sharp signals in the aromatic region; however, their corresponding ruthenium complexes exhibit slightly broader signals. The NMR spectrum of complex **5**, measured in $(CD_3)_2SO$ solution, shows four well resolved signals in the aromatic region, corresponding to the pyridyl and benzimidazole protons in which the two peripheral rings are magnetically equivalent. In an octahedral geometry, the tetradentate ligand (**L^1**) coordinates to a metal center in a plane, and the chloride ligands are in axial position. The lowest field broad singlet centered at δ 9.12 ppm is assigned to the H3 and H5 protons of the bipyridine. The doublets centered at δ 8.49 and 7.92 ppm are due to the Ha and Hd protons, respectively. The multiplet centered at δ 7.69 ppm is assigned to the Hb and Hc protons of the benzimidazole group.[33,34] In the aliphatic region, a singlet centered at δ 4.10 ppm is assigned to the methyl protons of the ester group.

In complex **6**, the H3 and H5 proton signals are separated and appear at δ 9.32 and 9.05 ppm, respectively. The doublets centered at δ 8.42 and 7.98 ppm are assigned to Ha and Hd protons, respectively. The multiplet centered at δ 7.69 ppm is assigned to the Hb and Hc protons of the benzimidazole group. The lowest field H3 singlet is very sensitive to the axial ligands, and its position can vary over a range of about 0.2 ppm in going from a chloro to a thiocyanato complex.

The ^{1}H NMR spectra of complexes **7** and **8** show well resolved features: two doublets and a doublet of doublets, which are assigned to the three magnetically inequivalent protons of the peripheral pyridine rings. The H3′ and H5′ protons of the central two pyridine rings exhibit two singlets (see Figure 1 for proton numbering scheme). The two doublets were assigned to the phenyl protons Ha and Hb, respectively. The complexes **9** and **10** show a similar pattern

(32) Nazeeruddin, M. K.; Zakeeruddin, S. M.; Humphry-Baker, R.; Jirousek, M.; Liska, P.; Vlachopoulos, N.; Shklover, V.; Fischer, C. H.; Graetzel, M. *Inorg. Chem.* **1999**, *38*, 6298.
(33) Mizushima, K.; Nakaura, M.; Park, S.-B.; Nishiyama, H.; Monjushiro, H.; Harada, K.; Haga, M.-A. *Inorg. Chim. Acta* **1997**, *261*, 175.
(34) Constable, E. C.; Elder, S. M.; Healy, J.; Tocher, D. A. *J. Chem. Soc., Dalton Trans.* **1990**, 1669.

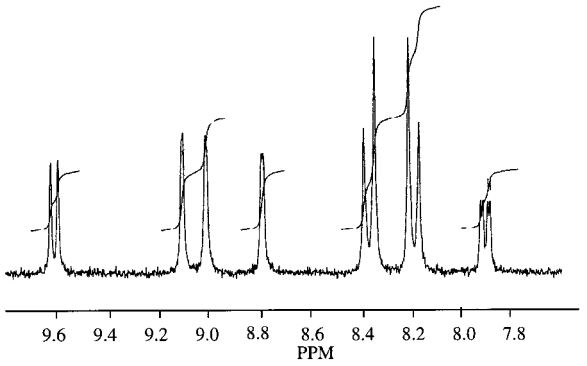

Figure 2. ^{1}H NMR spectrum of complex **7** in $(CD_3)_2SO$ at room temperature.

in the aromatic region, and a representative spectrum of complex **7** is shown in Figure 2. Complex **12** exhibits two singlets due to H3′ and H5′ protons of the central two pyridine rings. The two doublets and the two triplets were assigned to H3 and H6 and H4 and H5, respectively (see Figure 1 for proton numbering scheme). Complex **11** is insoluble even in DMSO at 60 °C for the purpose of measuring NMR spectra. The coordination induced chemical shift (CIS), $(\delta_{complex} - \delta_{ligand})$ is positive, which can be considered a measure of donor strength of the ligand.

(4.3) IR Spectral Data. Figure 3 shows the typical IR spectra of complexes **7** and **8** recorded as powders using ATR-FTIR in the 4000−400 cm^{-1} range. The spectra of all the compounds show a broad band at 3465 cm^{-1} due to υ(O−H) water molecules (not shown in Figure 3).[35] The complexes exhibited characteristic ring stretching modes in the region between 1620 and 1450 cm^{-1}. The major difference in the spectra of *trans*-dichloro complexes (Figure 3a) compared to that of *trans*-dithiocyanate complexes (Figure 3b) is the presence of a strong NCS band at around 2085 cm^{-1}, which is assigned to υ(CN) of the N-coordinated thiocyanate ligand.[36] The υ(CN) band shifted slightly to higher energy in complexes **6** (2100 cm^{-1}) and **10** (2092 cm^{-1}) compared to the band position in **8** (2085 cm^{-1}). The band due to υ(CN) is more intense than the band at 804 cm^{-1}, which is due to υ(CS).

Complexes **5** and **6** showed a peak at 1719 cm^{-1} due to the ester carbonyl group υ(CO). However, in **7** and **8**, the ester carbonyl band is observed at 1709 and 1703 cm^{-1}, respectively. The intense bands at 1277 and 1285 cm^{-1} are assigned to the υ(C−O) stretch in **7** and **8**, respectively. In these complexes, the methyl stretching modes are located at 2960 cm^{-1} and 3063 cm^{-1}.[37] The strong band at 1260 cm^{-1} in complexes **9** and **10** is assigned to the methoxy group υ(C−O) stretch.

(4.4) Electrochemical Studies. The electrochemical data for complexes **5**−**12** are listed in Table 1. The cyclic voltammogram of complex **5** measured in DMF solvent containing 0.1 M tetrabutylammonium tetrafluoroborate

Table 1. Cyclic Voltammetric Data Obtained for Complexes **5**−**12** in DMF Containing 0.1 M Tetrabutylammonium Tetrafluoroborate (TBATFB), V vs AgCl/Ag; $E_{1/2}$ Was Calculated as (Peak Potentials of $E^{ox}-E^{red})/2$

compound	$M^{III}-M^{II}$	ΔE (mV)	$M^{II}L/M^{II}L^-$	scan rate (mV S^{-1})
(**5**) [Ru(**L^1**)(Cl)$_2$]	0.40	60	−1.48[b]	500
(**6**) [Ru(**L^1**)(NCS)$_2$]	0.75[a]	80	−1.35[b]	500
(**7**) [Ru(**L^2**)(Cl)$_2$]	0.44	60	−1.46[b]	200
(**8**) [Ru(**L^2**)(NCS)$_2$]	0.79[a]	60	−1.2[b]	500
(**9**) [Ru(**L^3**)(Cl)$_2$]	0.36	60	−1.45[b]	500
(**10**) [Ru(**L^3**)(NCS)$_2$]	0.73[a]	75	−1.35[b]	500
(**11**) [Ru(**L^4**)(Cl)$_2$]	*c*			
(**12**) [Ru(**L^4**)(NCS)$_2$]	0.75[a]	75	−1.35[d]	1000

[a] The couple is quasireversible where the oxidation peak current is 4 times higher than the reduction peak current. [b] Irreversible. [c] Insoluble in DMF. [d] Quasireversible.

shows a chemically reversible wave at $E_{1/2} = 400$ mV (vs AgCl/Ag), which is attributed to the $Ru^{III/II}$ redox couple and is in good agreement with the reported value of 630 mV versus NHE for a very similar type of complex.[38] The separation between the cathodic and the anodic wave at a scan rate of 500 mV/s is 60 mV, and the ratio of peak currents is equal to 0.98. Complexes **7** and **9** show a reversible couple at 440 and 360 mV, respectively, assigned to the metal-centered oxidation processes. In these complexes, although the redox couples display a 60 mV separation, the i_{ox}/i_{red} peak current ratio is ∼1.5 probably arising from some chloride oxidation. The $Ru^{III/II}$ oxidation potential of complex **7** is more positive than that of dichloro complexes **5** and **9**. This reflects the increased electron-donating properties of ligands **L^1** and **L^3** compared to those of **L^2** due to the benzimidazole and methoxy donor groups. Complex **11** was insoluble for the purpose of obtaining reasonable concentrations for electrochemical studies.

The $Ru^{III/II}$ redox potentials of the thiocyanate complexes **6**, **8**, and **10** were more positive (by ≈350 mV) than their corresponding dichloro complexes and show quasireversible behavior (Table 1). This is in good agreement with the ligand electrochemical parameters scale,[14] according to which the thiocyanate $Ru^{III/II}$ wave should be ∼340 mV more positive than the dichloro species $Ru^{III/II}$ potential. The i_{ox}/i_{red} peak current is substantially greater than unity because of the oxidation of the thiocyanate ligand after the oxidation of the ruthenium(II) center. The standard equilibrium potential for thiocyanogen/thiocyanate couple is 0.53 V versus SCE in aqueous and nonaqueous solvents.[39] Surely, the standard equilibrium potential for coordinated thiocyanate shifts anodically compared to the thiocyanogen/thiocyanate couple because of electron donation to the metal. Nevertheless, the oxidation of metal at 0.75 V may still lead to the oxidation of thiocyanate ligand. It is interesting to note that the thiocyanate-containing ruthenium complexes are quite reversible, provided that the oxidation potential of the complex is around 0.5−0.6 V.[10b]

(35) Colthup, N. B.; Daly, L. H.; Wiberley, S. E. *Introduction to Infrared and Raman Spectroscopy*; Academic Press: New York, 1964; p 189.
(36) Wajda, S.; Rachlewicz, K. *Inorg. Chim. Acta*. **1978**, *31*, 35.
(37) *Infrared and Raman spectra of inorganic coordination compounds*, 5th ed.; Nakamoto, K., Ed.; Wiley International Publication: New York, 1997.
(38) Ryan, M. F.; Metcalfe, R. A.; Lever, A. B. P.; Haga, M.-A. *J. Chem. Soc., Dalton Trans.* **2000**, 2357.
(39) *Standard Potentials in Aqueous Solutions*; Bard, A. J., Parsons, R., Jordan, J., Eds.; Marcel Dekker: New York, 1985. (b) Bowmaker, G. A.; Kilmartin, A. P.; Wright, G. A. *J. Solid State Electrochem.* **1999**, *3*, 163.

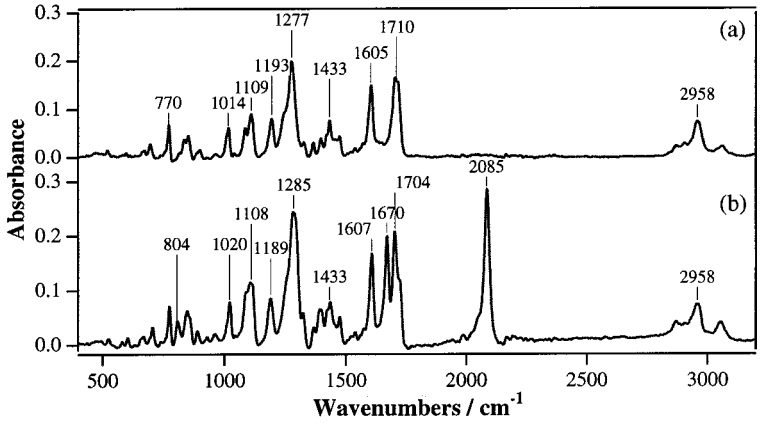

Figure 3. Infrared spectra of complexes **7** (a) and **8** (b).

Table 2. Electronic Spectral Data of Complexes **4**−**9** in DMF: Emission Spectra and Lifetime Data Were Obtained at 298 K by Exciting at the Lowest MLCT Maximum of the Complexes

trans complex	abs max (cm^{-1})[a] ($\epsilon/10^4$ M^{-1} cm^{-1})	em max (cm^{-1})[b]	τ (ns)
(**5**) [Ru(**L**^{1})$(Cl)_2$]	12 200 (0.16), 14 300 (sh) (0.36), 17 800 (0.75), 21 000 (0.76), 24 000 (sh) (0.88), 28 200 (sh) (2.13), 30 800 (3.03)	>10 500[c]	
(**6**) [Ru(**L**^{1})$(NCS)_2$]	12 500 (sh) (0.13), 15 400 (0.38), 19 000 (0.73), 22 200 (1.91), 27 500 (1.91), 29 400 (2.74)	11 100	
(**7**) [Ru(**L**^{2})$(Cl)_2$]	13 000 (sh) (0.48), 14 500 (0.88), 17 200 (0.89), 21 300 (0.99), 23 600 (1.15), 29 800 (2.17)	10 500[c]	
(**8**) [Ru(**L**^{2})$(NCS)_2$]	15 400 (0.83), 18 400 (0.74), 21 400 (0.75), 25 300 (1.03), 30 000 (2.12)	11 400	53
(**9**) [Ru(**L**^{3})$(Cl)_2$]	12 100 (sh) (0.12), 14 600 (0.99), 16 700 (0.75), 18 200 (sh), 20 800 (0.42), 25 000 (sh) (1.71), 29 900 (2.17)	>10 500[c]	
(**10**) [Ru(**L**^{3})$(NCS)_2$]	15 100 (1.01), 16 200 (1.16), 19 700 (0.72), 21 500 (0.6), 28 100 (4.79)	11 800	24
(**11**) [Ru(**L**^{4})$(Cl)_2$]	insoluble in DMF		
(**12**) [Ru(**L**^{4})$(NCS)_2$]	15 200 (0.98), 16 300 (1.10), 20 500 (1.43), 27 800 (2.89), 34 600 (4.67)	11 200	30
trans-[Ru$(dcbpyH_2)_2(Cl)_2$][d]	14 500 (0.60), 16 900 (0.84), 22 700 (0.80), 31 300 (2.78)	11 100	
trans-[Ru$(dcbpyH_2)_2(NCS)_2$][d]	17 200 (1.25), 18 900 (1.17), 24 900 (1.02), 31 800 (3.93)	11 500	12

[a] The values in parentheses are ±5%. [b] Weak and broad emission. [c] The true maxima is outside the spectral response of the photomultiplier used in our spectrofluorimeter, which is restricted to 10 500 cm^{-1}. [d] Reference 40.

In a cathodic scan, complexes **5**−**10** display reduction waves between −1.25 and −1.80 V; however, in the reverse scan, the reoxidation peak corresponding to the reduction wave is absent. These waves are assigned to the irreversible reduction of the tetradentate ligand. Complex **11** was insoluble in DMF, and complex **12** shows a quasireversible wave at −1.35 V (vs AgCl/Ag). The reduction potentials for the dithiocyanate complexes are shifted positively relative to the corresponding dichloro complexes (Table 1), but their irreversibility renders any discussion premature.

(4.5) Electronic Spectra. The *trans* complexes **5**−**12** are very weakly soluble in common organic solvents such as acetonitrile, ethanol, methanol, and dichloromethane. However, in DMF and DMSO, the complexes (except complex **11**) are soluble enough to measure the NMR, cyclic voltammetry, and electronic spectral properties. Figure 4 shows the UV−visible spectra of the *trans*-dichloro complexes **5**, **7**, and **9** measured in DMF as solvent. The absorption spectrum of complex **5** in DMF solution shows four broad absorption bands in the visible region shown in section 5.3 to be metal-to-ligand charge-transfer (MLCT). The band in the UV at 30 800 cm^{-1} with a shoulder at 28 200 cm^{-1} is assigned to an intraligand $\pi-\pi^*$ transition (Table 2). The spectral properties of complex **5** are similar to the analogous *trans* complex reported by Ryan et al.[38]

The absorption spectra of complexes **7** and **9** show bands covering the entire visible region from 25 000 to 11 800 cm^{-1} again with four broad bands assigned to MLCT transitions. The lowest energy MLCT bands of complexes **7** and **9** are

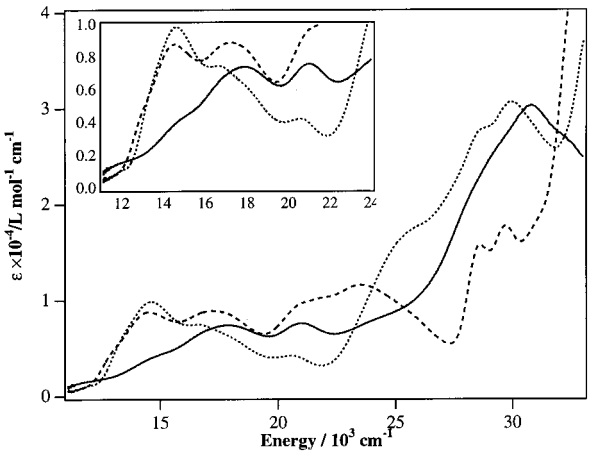

Figure 4. UV−vis absorption spectra of complexes **5** (solid line), **7** (dashed line), and **9** (dotted line), 5×10^{-5} M concentration in DMF solution.

significantly red-shifted compared to those of the *cis*-dichloro bis(2,2′-bipyridyl-4,4′-dicarboxylate) ruthenium(II) complex. However, there is excellent agreement between the visible spectra of **7** and **9** and the *trans*-dichloro bis(2,2′-bipyridyl-4,4′-dicarboxylate) ruthenium(II) complex where, in the latter complex, the absorption bands are observed in the visible region at 14 500, 16 900, and 22 700 cm^{-1} (Table 2).[40]

The *trans*-dithiocyanate complexes **6**, **8**, and **10** show MLCT bands (Figure 5) similar to those of the *trans*-dichloro

(40) Nazeeruddin, M. K.; Zakeeruddin, S. M.; Humphry-Baker, R.; Gorelsky, S. I.; Lever, A. B. P.; Grätzel, M. *Coord. Chem. Rev.* **2000**, *208*, 213−226.

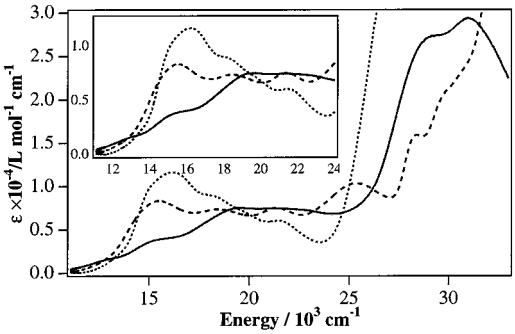

Figure 5. UV−vis absorption spectra of complexes **6** (solid line), **8** (dashed line), and **10** (dotted line), 5×10^{-5} M concentration in DMF solution.

complexes, but they are blue-shifted compared to the *trans*-dichloro complexes (Table 2), consistent with the relative increase in the $Ru^{III/II}$ oxidation potential.

(4.6) Emission Spectra. Table 2 shows the emission spectral data of *trans*-dichloro and dithiocyanato complexes obtained by exciting at 17 900 cm^{-1} at 298 K in DMF solution. The *trans*-dichloro complexes **5**, **7**, and **9** show onset of a weak emission above 10 500 cm^{-1}, and the true maxima are outside the spectral response of the photomultiplier used in our spectrofluorimeter. Complex **6** shows a weak emission onset at 11 100 cm^{-1}, which is slightly red-shifted compared to that of complexes **8**, **10**, and **12**. Complexes **8**, **10**, and **12**, when excited within the MLCT absorption band in an air-equilibrated DMF solution, show luminescence maxima at 11 400, 11 800, and 11 200 cm^{-1} and lifetimes of 53, 24, and 30(±1) ns, respectively. The emission spectral profile is independent of excitation wavelength, and the excitation spectrum matches well with the absorption spectrum. The red-shifted emission from complex **6** is due to better σ-donor properties of the benzimidazolyl unit causing lowering of the energy of the CT excited state.[41] The weakness of the emission could be accounted for by the proton-induced quenching due to the presence of H on the benzimidazole nitrogen.[42]

5. DFT and INDO/S Calculations

(5.1) Geometry Optimization. The structures of [Ru(L)-Cl_2] complexes were optimized with the B3LYP functional and using the LanL2DZ basis set. The structures of the complexes were optimized with no symmetry restraints. Geometry optimization of [Ru(**L**^{1})Cl_2] produced a structure with C_2 point group symmetry. Geometry optimizations of the complex of [Ru(**L**^{3})Cl_2] produced two structures with C_2 and C_s point group symmetries. These isomers have very close electronic energies ($E = 2 \times 10^{-3}$ eV) and differ by the relative position of the 3,4-(dimethoxy)phenyl groups with respect to each other. Their electronic structures and spectra are very similar. Because the isomer with C_2 symmetry has the lower energy, we continued our studies with this structure.

The complexes display a pseudooctahedral arrangement of ligands around the metal atom with the Cl−Ru−Cl angle of 172°. 2,2′:6′,2″:6″,2‴-Quaterpyridine in the optimized structure of [Ru(**L**^{3})Cl_2] is planar and has C_{2v} point group symmetry. However, the two 3,4-(dimethoxy)phenyl groups are out of the plane of the quaterpyridine ligand with a dihedral angle calculated to be 33°. The **L**^{1} ligand is not planar (and, thus, does not have C_{2v} point group symmetry) because of the buckling of the benzimidazole residues to minimize steric hindrance of the two hydrogen atoms. So, the actual symmetry of the ligand is C_2.

In all cases, the C_2 axis is defined as *z*, and the approximate plane of the ligand L is *xz*. The calculated Ru−Cl distances are 2.47−2.48 Å, somewhat shorter than those of a related complex, *trans*-[Ru(bpy)$_2$$Cl_2$], where the calculated (at the same level of theory) Ru−Cl distances are 2.508 Å. Both complexes, [Ru(**L**^{1})Cl_2] and [Ru(**L**^{3})Cl_2], demonstrate two sets of Ru−N distances, around 1.95 and 2.15−2.17 Å. These bond distances are in good agreement with the reported X-ray structures of ruthenium complexes with the 2,2′:6′,2″:6″,2‴-quaterpyridine ligand. For instance, in an X-ray structure of [Ru(L)Cl_2], where L is 5,5′,3″,5‴-tetramethyl-2,2′:6′,2″:6″,2‴-quaterpyridine, there are two sets of Ru−N distances (1.973−1.979 and 2.155−2.176 Å).[43] There is a marked difference between the Ru−N distances in these complexes and in *trans*-[Ru(bpy)$_2$$Cl_2$], in which the calculated (at the same level of theory) Ru−N distances are equal to 2.087 Å.

(5.2) Frontier Molecular Orbitals and Ruthenium−Ligand Coupling. The three highest occupied molecular orbitals (HOMO, HOMO − 1, and HOMO − 2) for [Ru(L)-Cl_2] complexes are mostly formed from 4d(Ru) orbitals.[44,45] Their contribution ranges from 52% to 84% for [Ru(**L**^{1})Cl_2] and from 62% to 88% for [Ru(**L**^{3})Cl_2] (Table 3). Other contributions to HOMO − 2, 1, 0 come almost entirely from π orbitals of the ligand L. The d_{yz} (*b*) Ru orbital directed toward the ligand L is coupled to the π orbitals of the ligand and is thereby delocalized to a considerable degree, greater than any other d(t_{2g}) orbital. The orbital energy splitting between HOMO and HOMO − 2, that is, overall splitting of d(t_{2g}), is greater for [Ru(**L**^{1})Cl_2] than for [Ru(**L**^{3})Cl_2] (0.35 and 0.21 eV respectively) and is consistent with a greater degree of metal−ligand coupling in the [Ru(**L**^{1})Cl_2] complex. The complexes with ligands **L**^{1} and **L**^{3} have a similar HOMO−LUMO gap of 5.3−5.4 eV.

The lowest unoccupied molecular orbitals are almost entirely localized on the ligand L but with a contribution of 4d(Ru) orbitals to LUMO and LUMO + 1 (so-called π-back-donation) which is twice as much for [Ru(**L**^{1})Cl_2] as for [Ru(**L**^{3})Cl_2]. The magnitude of the π-back-donation in [Ru(**L**^{1})Cl_2] is substantially larger than that calculated for the archetypical $[Ru(bpy)_3]^{2+}$ ion and comparable to that

(41) Nazeeruddin, M. K.; Muller, E.; Humphry-Baker, R.; Vlachopoulos, N.; Grätzel, M. *J. Chem. Soc., Dalton Trans.* **1997**, 4571.
(42) Kalyanasundaram, K.; Nazeeruddin, M. K. *Inorg. Chem.* **1990**, *29*, 1888.
(43) Chan, C.-W.; Lai, T.-F.; Che, C.-M. *J. Chem. Soc., Dalton Trans.* **1994**, 895.
(44) Gorelsky, S. I.; Dodsworth, E. S.; Lever, A. B. P.; Vlcek, A. A. *Coord. Chem. Rev.* **1998**, *174*, 469.
(45) Metcalfe, R. A.; Vasconcellos, L. C. G.; Mirza, H.; Franco, D. W.; Lever, A. B. P. *J. Chem. Soc., Dalton Trans.* **1999**, 2653. (b) Da Cunha, C. J.; Dodsworth, E. S.; Monteiro, M. A.; Lever, A. B. P. *Inorg. Chem.* **1999**, *38*, 5399. (c) Masui, H.; Freda, A. l.; Zerner, M. C.; Lever, A. B. P. *Inorg. Chem.* **2000**, *39*, 141.

Table 3. Frontier Molecular Orbitals (INDO/S) of *trans*-Ru(L)Cl_2 Complexes

orbital	Γ^a	ϵ (eV)^b	atomic orbital contribution (%) from Ru	ligand^c	Cl
		Ru($\mathbf{L^1}$)Cl_2 (C_2 point group)			
LUMO + 3	a (π^*)	−0.89	1	80 + 19	0
LUMO + 2	b (π^*)	−1.44	1	99 + 0	0
LUMO + 1	a (π^*-d_{xy})	−1.76	10	74 + 16	0
LUMO	b (π^*-d_{yz})	−1.99	19	68 + 10	3
HOMO	b ($d_{yz}-\pi$)	−7.26	52	43 + 2	3
HOMO − 1	a (d_{xy})	−7.41	67	29 + 1	3
HOMO − 2	a ($d_{z^2+x^2-y^2}$)	−7.61	84	14 + 0	2
HOMO − 3	a (π)	−8.31	2	97 + 0	1
HOMO − 4	b (π)	−8.52	7	91 + 0	2
		Ru($\mathbf{L^3}$)Cl_2 (C_2 point group)			
LUMO + 3	a (π^*)	−0.38	0	81 + 19	0
LUMO + 2	b (π^*)	−0.90	3	95 + 2	0
LUMO + 1	a (π^*-d_{xy})	−0.97	8	84 + 8	0
LUMO	b (π^*-d_{yz})	−1.27	10	82 + 6	2
HOMO	b ($d_{yz}-\pi$)	−6.65	62	30 + 4	4
HOMO − 1	a ($d_{z^2-x^2}$)	−6.80	88	11 + 0	1
HOMO − 2	a ($d_{xy}-\pi$)	−6.86	68	26 + 3	3
HOMO − 3	a (π)	−8.47	0	90 + 10	0
HOMO − 4	b (π)	−8.55	2	17 + 79	2

[a] Irreducible representation. For the *trans* isomer: z axis is Cl−Ru−Cl, x axis goes between $dcbpyH_2$ ligands. [b] Molecular orbital energy. [c] Contributions from the "main ligand" plus "functions" (L1, two methoxycarbonyl groups; L3, two 3,4-(dimethoxy)phenyl groups) (using DFT optimized geometries).

observed with the excellent π-acceptor ligand, *o*-diimino benzene (BQDI).[44] This degree of back-donation is also substantially larger than that calculated for the analogous 2,2′-bipyridine-6,6′-bis(2-*N*-dodecylbenzimidazoline) dichlororuthenium(II).[38]

The existence of low lying π^* orbitals, and the relatively low symmetry of these species, explains the presence of so many overlapping Ru d → π^* MLCT transitions in their electronic spectra. The carboxyl and dimethoxyphenyl functions of the ligands, $\mathbf{L^1}$ and $\mathbf{L^3}$, contribute up to 20% to the four low lying π^* orbitals but essentially make no contribution to the filled frontier orbitals (Table 2). According to the INDO/S calculations, there is only a small contribution of Cl^- ligand orbitals to the frontier molecular orbitals not exceeding 4%. Pictures of these frontier orbitals can be seen in the Supporting Information.

(5.3) Electronic Spectra. According to the INDO/S calculations, there are two groups of absorption bands in these complexes, one group lies in the visible region and one in the near-UV region. The [Ru($\mathbf{L^1}$)Cl_2] species is predicted to have four moderately strong MLCT transitions lying below 30 000 cm^{-1} with some $\pi \rightarrow \pi^*$ character especially at higher energy. The [Ru($\mathbf{L^3}$)Cl_2] has as many as seven lower lying MLCT bands of moderate to strong intensity. These clearly account for the generally broad and structured experimental absorption spectra of these species. Weaker and lower energy transitions cause some tailing to the red. The reasons for observing a combination of weak low-energy and stronger higher-energy transitions in the electronic spectra of complexes of this type have been discussed.[44]

The intense bands near 30 000 cm^{-1} are a result of internal $\pi \rightarrow \pi^*$ ligand and MLCT charge-transfer transitions

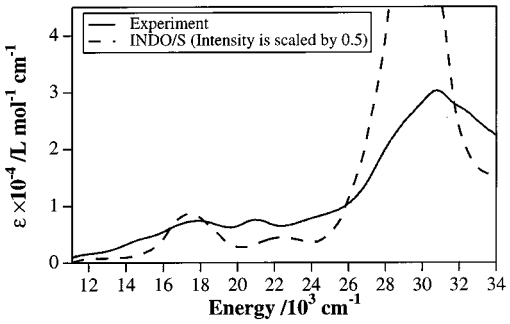

Figure 6. Experimental and simulated UV−vis absorption spectra of Ru($\mathbf{L^1}$)Cl_2.

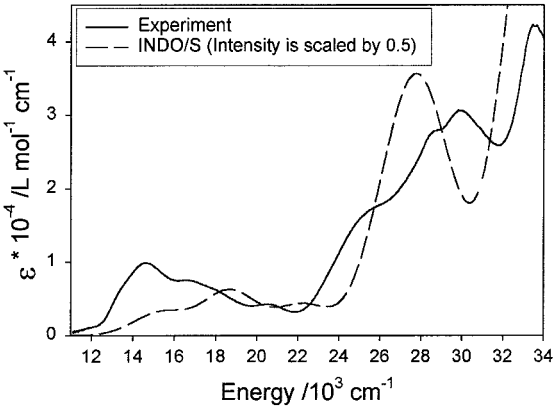

Figure 7. Experimental and simulated UV−vis absorption spectra of Ru($\mathbf{L^3}$)Cl_2.

(Table 4). The simulated electronic spectra are presented in Figures 6 and 7. Overall, there is good agreement between the experimental and predicted electronic spectra. INDO/S overestimates the intensities of calculated electronic transitions by a factor of 2 or so. A comparison between the calculated electronic spectra of [Ru($\mathbf{L^1}$)Cl_2] and analogous [Ru($\mathbf{L^{1x}}$)Cl_2], where $\mathbf{L^{1x}}$ is 6,6′-bis(1-*H*-benzimidazol-2-yl)-2,2′-bipyridine, shows that the removal of two methoxycarbonyl functions does not affect the main features of the electronic spectrum of this complex. However, it does affect the intense band near 30 000 cm^{-1} significantly.[38]

The complexity and substantial number of MLCT transitions cause a very broad band absorption of light across the visible region, making these species particularly important for the sensitization function they are designed to facilitate.

6. Photovoltaic Measurements

Dye solutions of complexes **6**, **8**, **10**, and **12** were prepared in ethanol (2×10^{-4} M). TiO_2 electrodes, which were treated with titanium tetrachloride solution,[10b] were heated to 500 °C at a rate of 35 °C/min under oxygen, left at this temperature for 10 min, and then allowed to cool to ≈ 100 °C. The hot electrodes were immersed into the dye solutions for 20 h at 25 °C. The TiO_2 electrodes were not colored under these conditions. Then, the solutions containing TiO_2 electrodes were subjected to reflux conditions for 12 h. Surprisingly, the electrodes were still colorless, suggesting that the ester functional groups were not suitable for anchoring onto the TiO_2 surface. Moreover, our experiment ascertains that the ester groups were quite stable (not

Table 4. Comparison between Experimental and Calculated (INDO/S) Electronic Spectra of *trans*-Ru(L)Cl_2 Complexes

expt	calcd		
$h\nu$/1000 cm^{-1}	$h\nu$/1000 cm^{-1}	f [b]	assignment[a,c]
	Ru(**L**[1])Cl_2 (C_2 point group) LUMO = 105		
	10.9	0.0047	H − 1 → L (55%), H − 2 → L (39%) MLCT
12.2, 14.3 (sh)	12.7	0.018	H − 2 → L (55%), H − 1 → L (−37%) MLCT
17.8	17.4	0.24	H → L + 1 (85%) MLCT
	20.2	0.020	H → L + 2 (71%) MLCT
21.0	22.3	0.091	H − 1 → L + 2 (81%) MLCT
24.0 (sh)	26.6	0.14	H − 3 → L (62%) $\pi \rightarrow \pi^*$
28.2 (sh)	28.0	0.34	H → L + 3 (76%) MLCT
	29.3	0.050	H − 4 → L + 10 (68%) $\pi \rightarrow \pi^*$
30.8	29.7	1.7	H − 4 → L (22%), H − 3 → L + 1 (21%) $\pi \rightarrow \pi^*$
	Ru(**L**[3])Cl_2 (C_2 point group) LUMO = 121		
12.1 (sh)	12.8	0.0001	H − 1 → L (92%) MLCT
14.6	15.1	0.047	H − 2 → L (86%) MLCT
16.7	15.7	0.041	H → L (65%) MLCT
18.2 (sh)	18.6	0.15	H → L + 1 (90%) MLCT
	19.6	0.017	H → L + 2 (45%), H − 1 → L + 9 (27%) MLCT
20.8	22.3	0.11	H − 2 → L + 2 (82%) MLCT
25.0 (sh)	25.6	0.087	H − 2 → L + 1 (39%), H → L + 4 (22%) MLCT
	26.8	0.44	H → L + 3 (77%) MLCT
29.9	28.1	0.44	H − 2 → L + 3 (64%) MLCT
	28.8	0.24	H − 2 → L + 4 (26%), H − 3 → L (25%), H → L + 5 (22%) MLCT

[a] H = HOMO; L = LUMO. [b] Oscillator strength. [c] Only the major parent one-electron excitations are reported. Their percentage contributions to wave functions of excited states are given in parentheses (using DFT optimized geometries).

hydrolyzed) even under reflux conditions in the presence of TiO_2 electrodes. Therefore, hydrolysis of the ester groups of the complexes is required in order to anchor onto the semiconductor surface.

Complex **12** was hydrolyzed using the following method: 25 mg of complex **12** was taken into 10 mL of DMF to which was added 5 mL of triethylamine and 10 mL of H_2O. Then, the solution was refluxed for 24 h, and the solvents were removed using a rotary evaporator. A 15 mL portion of H_2O was added to the resulting residue that gave a precipitate, which was filtered and dried under vacuum at 50 °C. The ^1H NMR (in CD_3OD) data show the absence of ethyl protons, indicating complete hydrolysis of the ester groups. The solution of hydrolyzed complex **12** was prepared by first dissolving in 5% DMSO and then diluting with 95% ethanol. The typical concentrations of solutions were 3×10^{-4} M. The heated TiO_2 electrodes were plunged into the dye solution for 15 h at 25 °C.

In contrast to the ester solutions, when the TiO_2 electrodes were dipped into the solution of hydrolyzed complex **12**, the electrodes were intensely colored. Figure 8 shows absorption spectra of hydrolyzed complex **12** anchored onto 6 μm thick TiO_2 nanocrystalline electrode, which are very similar to the solution spectra.

The initial studies of the films sensitized by hydrolyzed complex **12** into a photoelectrochemical "sandwich" solar cell employing an electrolyte that contains 0.6 M dimethylpropylimidazolium iodide, 0.1 M iodine, 0.5 M *tert*-butylpyridine, and 0.1 M lithium iodide in methoxyacetonitrile were performed. Figure 9 shows the photocurrent action spectrum of such a cell where the incident photon to current conversion efficiency is plotted as a function of wavelength. A broad feature appears covering the entire visible spectrum and extending into the near-IR region up to 940 nm. The incident photon-to-current conversion efficiency (IPCE) value

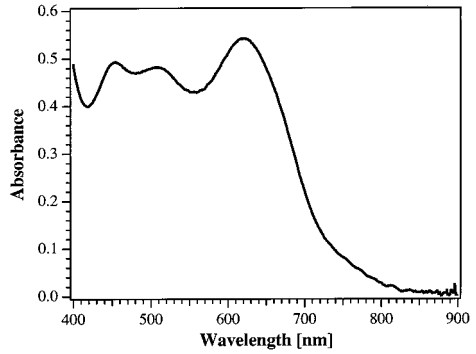

Figure 8. Absorption spectra of hydrolyzed complex **12** anchored onto 6 μm thick TiO_2 nanocrystalline electrode after subtracting the blank (similar 6 μm thick TiO_2 nanocrystalline electrode was used as a blank).

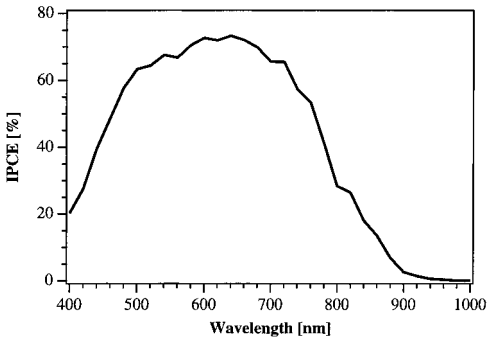

Figure 9. Photocurrent action spectrum obtained with the hydrolyzed complex **12** attached to nanocrystalline TiO_2 films. The incident photon to current conversion efficiency is plotted as a function of the wavelength of the exciting light.

in the plateau region is about 75%. The overlap integral of this curve with the standard global AM 1.5 solar emission spectrum yields a short circuit photocurrent density (isc) of 18 ± 0.5 mA/cm^2. The open circuit potential (Voc) is 650 ± 50 mV, and the fill factor (ff) is 0.65 ± 0.05.

The reported values are preliminary and were not optimized for the current, open circuit potential, and fill factor. The current and the open circuit potential of the cell depend on the number of protons carried by the sensitizer, and the fill factor depends to a large degree on current collection geometry and the viscosity of the electrolyte employed. Currently, these parameters are being scrutinized in our laboratory. A current of 18 mA/cm^2 for 12 μm thick TiO_2 electrodes under AM 1.5 solar emission spectrum is really impressive. Therefore, we believe that the panchromatic light harvesting properties of these complexes combined with nearly quantitative electron injection from the excited dye into the conduction band of the nanocrystalline TiO_2 film should supersede that of the N3 sensitizer after optimization of the open circuit potential and the fill factor.

7. Conclusions and Perspectives

The noteworthy feature of this work is success in developing anchoring panchromatic sensitizers based on ruthenium, which display absorption bands in the entire visible and near-IR region, see especially inserts to Figures 4 and 5. The enhanced spectral response of these complexes compared to that of the widely used N3 dye is expected to improve significantly the overall efficiency of a dye-sensitized solar cell. The current of 18 mA/cm^2 for 12 μm thick TiO_2 cell using hydrolyzed complex **12** under AM 1.5 solar emission spectrum testifies that our point is made. Thus, this class of compounds serves as the basis for the design of new compounds containing anchoring phenyl and diphenyl substituents on the 4,4′,4″,4‴-positions of 2,2′:6′,2″:6″,2‴-quaterpyridine. Variation in the phenyl substitution should permit us to increase the molar extinction coefficient allowing a reduction in film thickness, which should benefit the open circuit potential and overall efficiency of the solar cells. We are currently addressing the research directed toward this goal in our laboratory.

Acknowledgment. We acknowledge financial support of this work by the Swiss Science Foundation, Swiss Federal Office for Energy (OFEN), the Institute for Applied Photovoltaics (INAP, Gelsenkirchen, Germany), and the Natural Sciences and Engineering Research Council (Ottawa). We also acknowledge the Province of Ontario (Canada) for a Ontario Graduate Fellowship for S.I.G. We thank Dr. P. Liska, Dr. M. Jirousek, and P. Comte for their excellent assistance with the laboratory work. We are grateful to Dr. R. Houriet, Department of Materials Science, Swiss Federal Institute of Technology, for his assistance in measuring the ATR-FTIR spectra.

Supporting Information Available: Structures of [Ru(**L**^{1})Cl_2] and [Ru(**L**^{3})Cl_2] and pictures of the frontier orbitals. This material is available free of charge via the Internet at http://pubs.acs.org.

IC010512U